Table 2 The list of 97 genes elevated in human colorectal tumor tissues

No	Gene	Description	Accession no.	Log_2 ratio (tumor/normal)
1	*COL1A1*	Collagen, type I, α1	NM_000088	2.137
2	*SPP1*	Secreted phosphoprotein 1 (osteopontin, bone sialoprotein I, early T-lymphocyte activation 1)	NM_000582	1.531
3	*CCL20*	Chemokine (C-C motif) ligand 20	NM_004591	1.501
4	*UBD*	Ubiquitin D	NM_006398	1.392
5	*TGFBI*	Transforming growth factor, β-induced, 68 kDa	NM_000358	1.345
6	*IFITM1*	Interferon induced transmembrane protein 1 (9–27)	NM_003641	1.341
7	*MMP12*	Matrix metallopeptidase 12 (macrophage elastase)	NM_002426	1.248
8	*CEACAM6*	Carcinoembryonic antigen-related cell adhesion molecule 6 (non-specific cross reacting antigen)	NM_002483	1.237
9	*RPS21*	Ribosomal protein S21	NM_001024	1.232
10	*PFDN4*	Prefoldin 4	NM_002623	1.209
11	*TIMP1*	TIMP metallopeptidase inhibitor 1	NM_003254	1.191
12	*NEK6*	NIMA (never in mitosis gene a)-related kinase 6	NM_014397	1.089
13	*MMP1*	Matrix metallopeptidase 1 (interstitial collagenase)	NM_002421	1.079
14	*S100A11*	S100 calcium binding protein A11 (calgizzarin)	NM_005620	1.055
15	*IFNAR1*	Interferon (α, β and ω) receptor 1	NM_000629	1.031
16	*CPSF4*	Cleavage and polyadenylation specific factor 4, 30 kDa	NM_006693	1.024
17	*TMEPAI*	Transmembrane, prostate androgen induced RNA	NM_020182	1.013
18	*RPL31*	Ribosomal protein L31	NM_000993	0.995
19	*CPNE3*	Copine III	NM_003909	0.988
20	*UBE2C*	Ubiquitin-conjugating enzyme E2C	NM_007019	0.979
21	*NQO1*	NAD(P)H dehydrogenase, quinone 1	NM_000903	0.968
22	*MYC*	V-myc myelocytomatosis viral oncogene homolog (avian)	NM_002467	0.966
23	*LCN2*	Lipocalin 2 (oncogene 24p3)	NM_005564	0.959
24	*PRKAA1*	Protein kinase, AMP-activated, α1 catalytic subunit	NM_006251	0.958
25	*GNGT2*	Guanine nucleotide binding protein (G protein), gamma transducing activity polypeptide 2	NM_031498	0.932
26	*PSMA7*	Proteasome (prosome, macropain) subunit, α-type, 7	NM_002792	0.932
27	*SLC3A2*	Solute carrier family 3 (activators of dibasic and neutral amino acid transport), member 2	NM_002394	0.925
28	*C10ORF137*	Chromosome 10 open reading frame 137	NM_015608	0.917
29	*CKS2*	CDC28 protein kinase regulatory subunit 2	NM_001827	0.912
30	*RPS6*	Ribosomal protein S6	NM_001010	0.911
31	*RPL39*	Ribosomal protein L39	NM_001000	0.910
32	*COL10A1*	Collagen, type X, α1(Schmid metaphyseal chondrodysplasia)	NM_000493	0.910
33	*MLLT1*	Myeloid/lymphoid or mixed-lineage leukemia (trithorax homolog, Drosophila); translocated to, 1	NM_005934	0.896
34	*GABRD*	γ-aminobutyric acid (GABA) A receptor, δ	NM_000815	0.895
35	*COL1A2*	Collagen, type I, α2	NM_000089	0.894
36	*DKFZP564O0463*	WD repeats and SOF1 domain containing	NM_015420	0.894
37	*RIPK2*	Receptor-interacting serine-threonine kinase 2	NM_003821	0.893

(Continued)

Table 2 *(Continued)*

No	Gene	Description	Accession no.	Log_2 ratio (tumor/normal)
38	*FOXM1*	Forkhead box M1	NM_021953	0.892
39	*PIGL*	Phosphatidylinositol glycan, class L	NM_004278	0.870
40	*NIN*	Ninein (GSK3B interacting protein)	NM_016350	0.870
41	*ATP2B1*	ATPase, Ca^+ transporting, plasma membrane 1	NM_001682	0.870
42	*MIF*	Macrophage migration inhibitory factor (glycosylation-inhibiting factor)	NM_002415	0.861
43	*PCYOX1*	Prenylcysteine oxidase 1	NM_016297	0.850
44	*ARF4*	ADP-ribosylation factor 4	NM_001660	0.843
45	*MEOX2*	Mesenchyme homeo box 2 (growth arrest-specific homeo box)	NM_005924	0.840
46	*HTR2B*	5-hydroxytryptamine (serotonin) receptor 2B	NM_000867	0.836
47	*HRASLS3*	HRAS-like suppressor 3	NM_007069	0.827
48	*GYPA*	Glycophorin A (includes Ss blood group)	NM_002099	0.819
49	*GDF15*	Growth differentiation factor 15	NM_004864	0.817
50	*NPHS2*	Nephrosis 2, idiopathic, steroid-resistant (podocin)	NM_014625	0.816
51	*FIBL-6*	Hemicentin 1	NM_031935	0.804
52	*AKAP8L*	A kinase (PRKA) anchor protein 8-like	NM_014371	0.787
53	*SLC12A2*	Solute carrier family 12 (sodium/potassium/ chloride transporters), member 2	NM_001046	0.784
54	*CDK10*	Cyclin-dependent kinase (CDC2-like) 10	NM_003674	0.781
55	*UFM1*	Ubiquitin-fold modifier 1	NM_016617	0.780
56	*TBX19*	T-box 19	NM_005149	0.775
57	*DPEP1*	Dipeptidase 1 (renal)	NM_004413	0.775
58	*NNMT*	Nicotinamide N-methyltransferase	NM_006169	0.754
59	*RPS20*	Ribosomal protein S20	NM_001023	0.748
60	*ZNF84*	Zinc finger protein 84 (hpf2); znf84	NM_003428	0.740
61	*HIG2*	Hypoxia-inducible protein 2	NM_013332	0.639
62	*SNAI2*	Snail homolog 2 (Drosophila)	NM_003068	0.610
63	*SLAMF7*	SLAM family member 7	NM_021181	0.604
64	*RAN*	RAN, member RAS oncogene family	NM_006325	0.603
65	*SNAI1*	Snail homolog 1 (Drosophila)	NM_005985	0.580
66	*MRAS*	Muscle RAS oncogene homolog	NM_012219	0.543
67	*ARHGEF4*	Rho guanine nucleotide exchange factor (GEF) 4	NM_015320	0.536
68	*MDK*	midkine (neurite growth-promoting factor 2)	NM_002391	0.530
69	*BRAF*	Y-raf murine sarcoma viral oncogene homolog B1	NM_004333	0.528
70	*FBXO11*	F-box protein 11	NM_012167	0.519
71	*AATF*	Apoptosis antagonizing transcription factor	NM_012138	0.516
72	*FIGN*	Fidgetin	NM_018086	0.506
73	*MMP9*	Matrix metallopeptidase 9 (gelatinase B, 92kDa gelatinase, 92kDa type IV collagenase)	NM_004994	0.497
74	*VEGFA*	Vascular endothelial growth factor	NM_003376	0.496
75	*FBXW5*	F-box and WD-40 domain protein 5	NM_178225	0.481
76	*LTA*	Lymphotoxin α (TNF superfamily, member 1)	NM_000595	0.476
77	*TRAP1*	TNF receptor-associated protein 1	NM_016292	0.455
78	*LGALS1*	Lectin, galactoside-binding, soluble, 1 (galectin 1)	NM_002305	0.453
79	*RRAS*	Related RAS viral (r-ras) oncogene homolog	NM_006270	0.441
80	*MMP10*	Matrix metallopeptidase 10 (stromelysin 2)	NM_002425	0.440

(Continued)

Table 2 (*Continued*)

No	Gene	Description	Accession no.	Log_2 ratio (tumor/normal)
81	*FBXW11*	F-box and WD-40 domain protein 11	NM_012300	0.440
82	*SAT*	Spermidine/spermine N1-acetyltransferase	NM_002970	0.440
83	*RPN2*	Ribophorin II	NM_002951	0.400
84	*RAB4B*	RAB4B, member RAS oncogene family	NM_016154	0.398
85	*FETUB*	Fetuin B	NM_014375	0.395
86	*ELF4*	E74-like factor 4 (ets domain transcription factor)	NM_001421	0.388
87	*SHAX3*	Chromatin modifying protein 4C	NM_152284	0.387
88	*ECT2*	Epithelial cell transforming sequence 2 oncogene	NM_018098	0.384
89	*HES6*	Hairy and enhancer of split 6 (Drosophila)	NM_018645	0.383
90	*DDEF1*	Development and differentiation enhancing factor 1	NM_018482	0.378
91	*RHEB*	Ras homolog enriched in brain	NM_005614	0.375
92	*CTNND1*	Catenin (cadherin-associated protein), δ1	NM_001331	0.368
93	*DNMT3B*	DNA (cytosine-5-)-methyltransferase 3β	NM_006892	0.365
94	*ASPM*	ASP (abnormal spindle)-like, microcephaly associated (Drosophila)	NM_018136	0.360
95	*PCDHA10*	Protocadherin α10	NM_018901	0.349
96	*VEGFC*	Vascular endothelial growth factor C	NM_005429	0.347
97	*RASGRF1*	Ras protein-specific guanine nucleotide-releasing factor 1	NM_002891	0.346

siRNAs using reverse transfection-based cell transfection array. To evaluate the efficiency of the cell transfection array, we used GAPDH siRNA against the gene encoding GAPDH (glyceraldehyde-3-phosphate dehydrogenase). GAPDH siRNA transfer caused an approximate 75% reduction of the GAPDH mRNA expression in HT-29 cells relative to the control nontargeting siRNA (data not shown).

We assessed siRNAs for their ability to induce apoptosis in HT-29 compared with the control nontargeting siRNA. We measured cell viability by resazurin reduction and examined apoptosis by caspase-3/7 activity. Caspase-3/7 activity was normalized by viable cell number (measurement value of resazurin reduction) and Caspase-3/7 activation by siRNAs was compared with control nontargeting siRNA. The results indicated that the downregulation of 11 genes (*TIMP1*, *S100A11*, *TMEPAI*, *PSMA7*, *COL10A1*, *RAN*, *VEGFA*, *LTA*, *TRAP1*, *MMP10*, and *RHEB*) resulted in a marked induction of apoptosis in HT-29 cells (caspase-3/7 activity, percentage of nontargeting siRNA > 200, $P < 0.05$, Figure 2). In particular, the PSMA7 siRNA pool and the RAN siRNA pool strongly enhanced caspase-3/7 activity (caspase-3/7 activity, percentage of nontargeting siRNA > 300, $P < 0.001$, Figure 2). We validated these results by counting Hoechst-stained cells showing apoptotic nuclear condensation and fragmentation (Figure 3A) and found that there was a significantly higher apoptotic cell death rate in cells given PSMA7 siRNA pool and RAN siRNA pool relative to that in cells given control siRNA ($P < 0.01$, Figure 3B). At 72 hours after treatment with siRNA, there was substantial cell death induced by the PSMA7 siRNA pool and the RAN siRNA pool compared with the control nontargeting siRNA (Figure 3C).

We assessed the efficacy of PSMA7 siRNA pool and RAN siRNA pool for the knockdown of mRNA by cell-direct real-time RT-PCR analysis. This analysis revealed that PSMA7 siRNA pool and RAN siRNA pool inhibited the mRNA expression relative to the control nontargeting siRNA, 80% and 60% respectively (Figure 3D). To evaluate the knockdown efficiency of individual siRNAs of the siRNA pool, we performed a liposome-mediated siRNA transfection. PSMA7 siRNA #2 and RAN siRNA #4 most efficiently silenced PSMA expression (70% reduction of mRNA) and RAN expression (70% reduction of mRNA), respectively (Figure 3E). We also confirmed that PSMA7 siRNA #2 and RAN siRNA #4 strongly increased caspase-3/7 activity in HT-29 cells (data not shown). PSMA7 siRNA #2 and RAN siRNA #4 were used in further *in vivo* experiments.

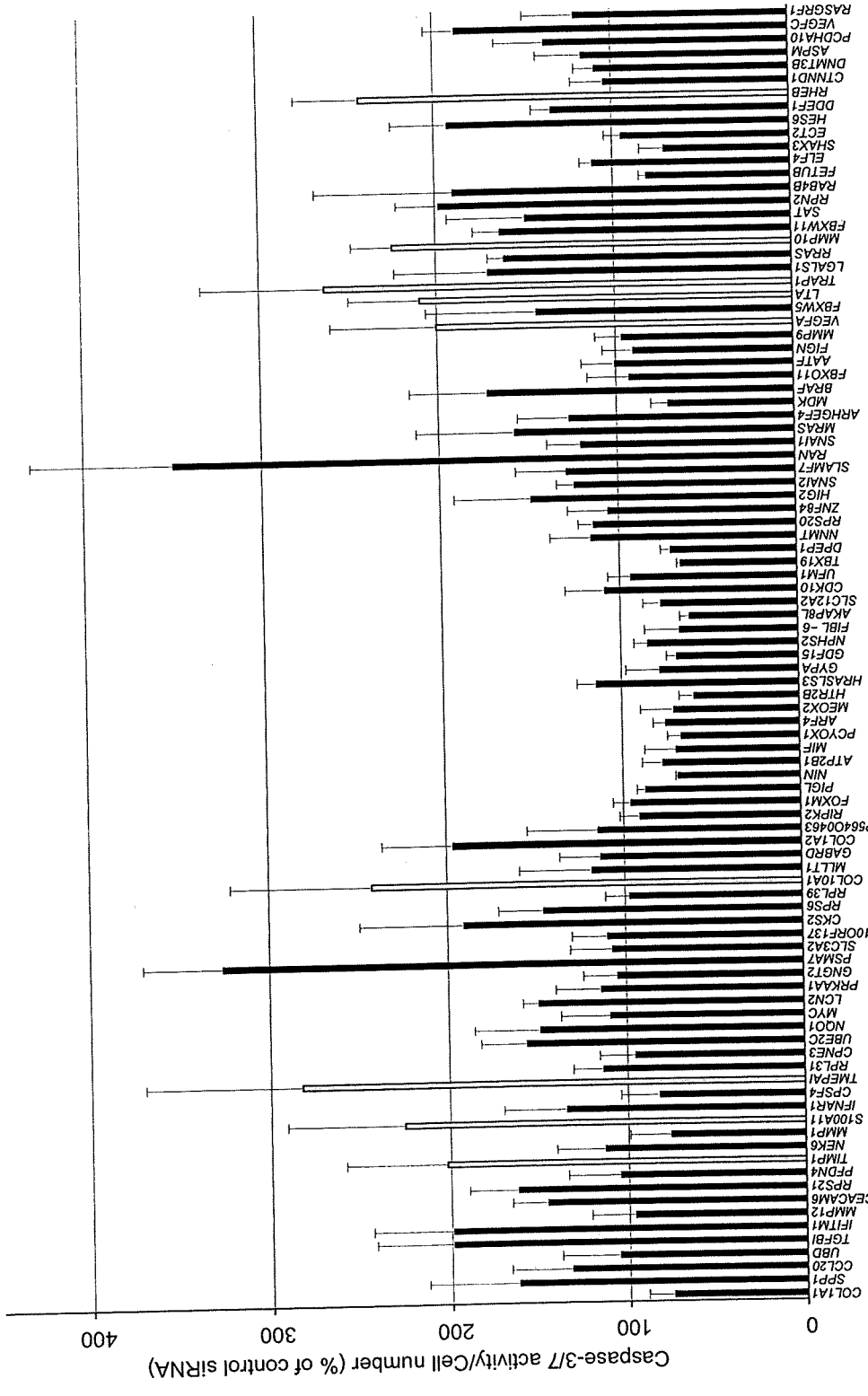

Figure 2 Functional screening of genes by RNAi-cell transfection array in cultured colorectal cancer cells. Cell number and caspase-3/7 activity were measured 72 hours after transfection of HT-29 cells. Caspase-3/7 activity was normalized by viable cell number to evaluate apoptosis induction. Control nontargeting siRNA is set to 100% and relative activity is shown. Yellow color bar: relative activity (%) >200, $P < 0.05$; blue color bar: relative activity (%) >300, $P < 0.001$. $n = 4$ per group. Values are mean ± SD.

Abbreviations: SD, standard deviation; siRNA, small interfering RNAs.

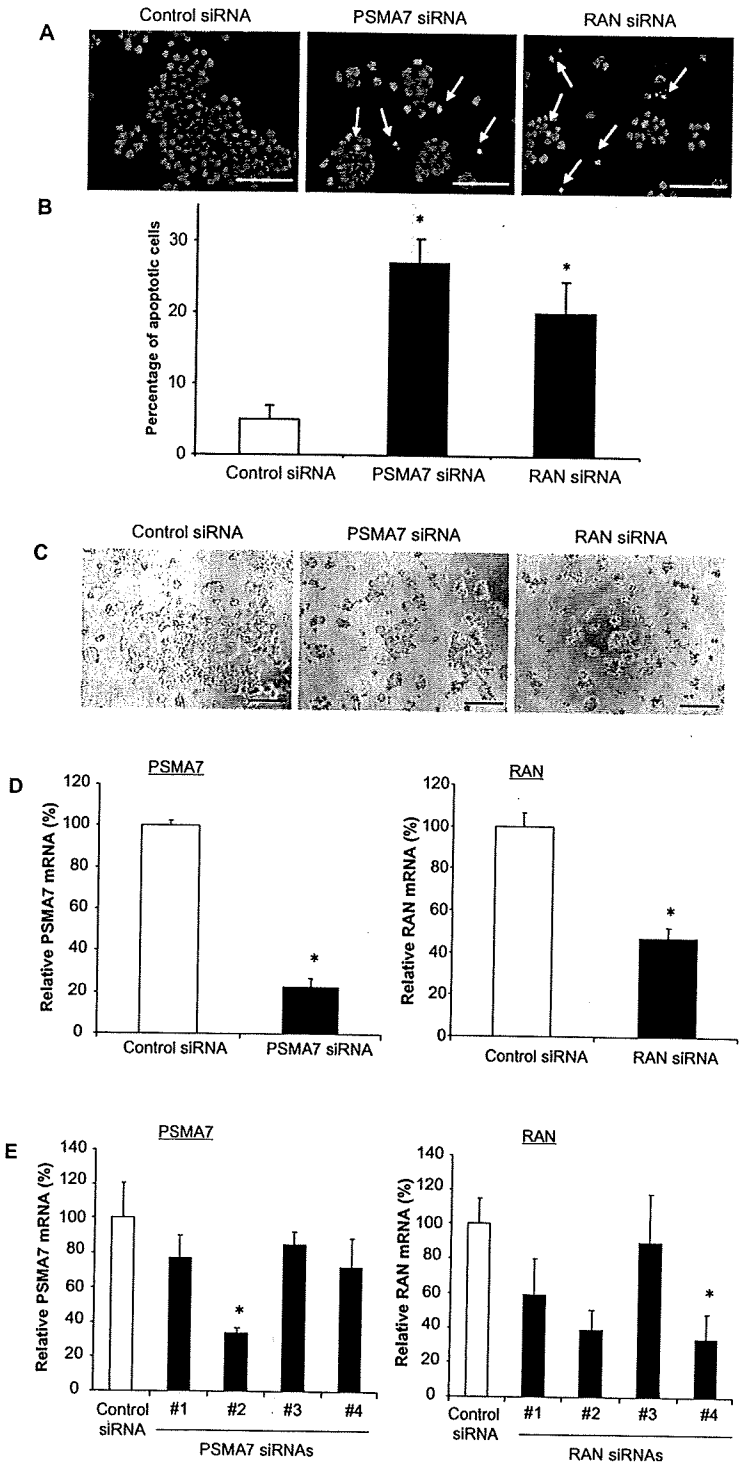

Figure 3 Apoptosis of HT-29 cells transduced with PSMA7 siRNA and RAN siRNA. **A)** Hoechst staining of cells 72 hours after the transfection of siRNA. Scale bar, 100 μm. The arrows indicate cells with nuclear condensation and fragmentation. **B)** Numbers of apoptotic cells from (A). The data show the percentage of apoptotic cells. As a control, nontargeting control siRNA was used ($n = 4$ per group, $^*P < 0.01$). **C)** Phase contrast micrograph of HT-29 cells 72 hours after the treatment of siRNA. Scale bar, 200 μm. **D)** Knockdown of mRNA by PSMA7 siRNA pool and RAN siRNA pool using cell transfection array was measured 72 hours after transfection. ($n = 5$ per group, $^*P < 0.001$). **E)** Knockdown of mRNA by PSMA7 siRNAs and RAN siRNAs. Expression of PSMA7 mRNA and RAN mRNA was measured 72 hours and 48 hours after transfection, respectively ($n = 3$ per group, $^*P < 0.01$). As a control, nontargeting siRNA was used. Values are mean ± SD.

Abbreviations: PSMA7, proteasome subunit, α-type, 7; RAN, ras-related nuclear protein; SD, standard deviation; siRNA, small interfering RNAs.

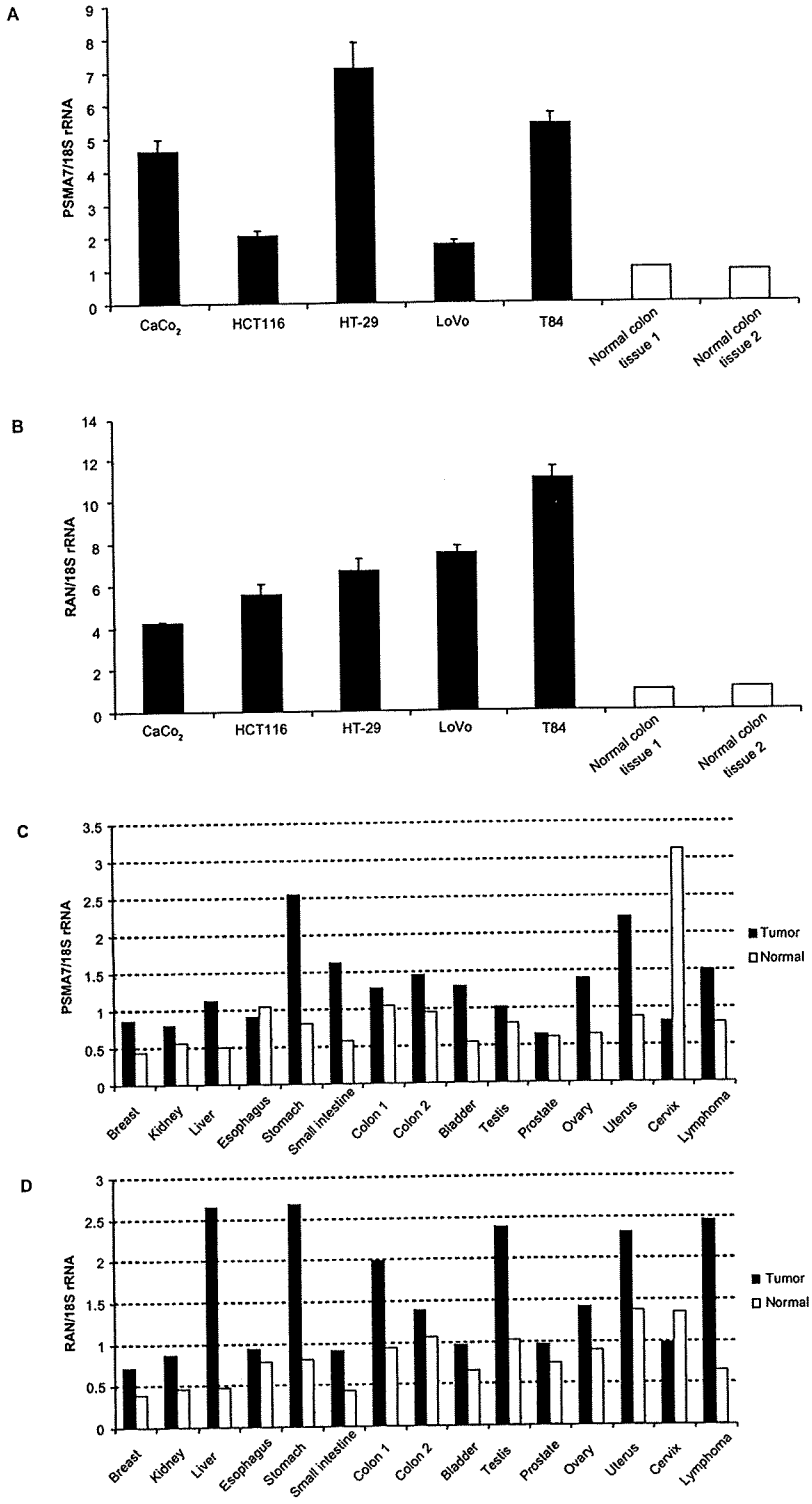

Figure 4 *PSMA7* and *RAN* expression in colorectal cancer cell lines and tumor tissues. PSMA7 mRNA and RAN mRNA expression were analyzed by real-time RT-PCR. **A)** PSMA7 mRNA expression in colorectal cancer cell lines. $n = 3$ per group. Values are mean ± SD. **B)** RAN mRNA expression in colorectal cancer cell lines. $n = 3$ per group. Values are mean ± SD. **C)** PSMA7 mRNA expression in various tumor tissues (■, $n = 1$) and their normal adjacent tissues (□, $n = 1$). **D)** RAN mRNA expression in various tumor tissues (■, $n = 1$) and their normal adjacent tissues (□, $n = 1$). mRNA expression was normalized to 18S rRNA. Mean of normal colon tissues is set to 1.
Abbreviations: PSMA7, proteasome subunit, α-type, 7; RAN, ras-related nuclear protein; RT-PCR, reverse transcriptase-polymerase chain reaction; SD, standard deviation.

Thus, downregulation of PSMA7 and RAN expression by siRNA induces apoptosis in colon cancer cells, results that suggest that PSMA7 and RAN might act as a suppressor of apoptosis in colorectal cancer.

Overexpression of PSMA and RAN in colorectal cancer cell lines and tumor tissues

To investigate the role of PSMA and RAN in colorectal cancer, we analyzed the mRNA expression levels of PSMA7 and RAN by real-time RT-PCR. PSMA7 and RAN mRNA were significantly highly expressed in colorectal cancer cell lines Caco-2 (human colorectal adenocarcinoma), HCT116 (human colorectal carcinoma), HT-29 (human colorectal adenocarcinoma), LoVo (human colorectal adenocarcinoma, derived from supraclavicular lymph node metastatic site) and T84 (human colorectal carcinoma, derived from lung metastatic site), compared with normal colon tissues (Figures 4A, 4B). mRNA expression levels of PSMA7 and RAN in human tumoral colon tissues were higher than those of normal adjacent colon tissues (Figures 4C, 4D). These results indicate that PSMA7 and RAN strongly correlated with colorectal tumorigenesis and malignancy.

Furthermore, PSMA7 was overexpressed in other tumor tissues, especially uterus, stomach, and small intestine tumor tissues (Figure 4C). Similarly, RAN was overexpressed in other tumor tissues, in particular uterus, liver, testis, and stomach tumors and lymphoma tissues (Figure 4D). Thus, PSMA7 and RAN were overexpressed in not only colon tumor tissues but also in other tumor tissues, and PSMA7 and RAN might be involved in the development of multiple cancers.

Correlation of PSMA7 and RAN expression with liver and lung metastases in human colorectal cancer

We next investigated the levels of *PSMA7* and *RAN* expression in human colorectal cancers. The results are summarized in Table 3. PSMA7 showed a borderline significance ($P = 0.076$) for correlation with liver metastasis in colorectal cancer patients. In contrast, no significant correlation between the PSMA7 expression and lung metastasis was found in patients ($P = 0.534$). Decreased expression of RAN showed a significance ($P = 0.023$) for correlation with lung metastasis; however, there is no correlation with liver metastasis ($P = 0.911$). However, to know whether or not the levels of *PSMA7* and *RAN* expression showed correlation with any other clinicopathological features such as depth of invasion, tumor size, lymphatic invasion, or the presence of lymph node metastasis, further analysis is needed.

PSMA7 siRNA and RAN siRNA induce apoptosis *in vivo*

To extend our *in vitro* findings and to determine whether PSMA7 and RAN could be effective therapeutic targets for colorectal cancer, we examined the effect of PSMA7 siRNA and RAN siRNA on an animal model of colon tumors by subcutaneously implanting HT-29 cells into mice. We injected the PSMA7 siRNA #2, RAN siRNA #4, or nontargeting control siRNA (1 nmol per tumor) into tumors that had reached 5–6 mm in diameter seven days after inoculation of HT-29 cells. The mRNA levels of PSMA7 and RAN in the tumors given siRNA were measured. mRNA expression was significantly reduced in mouse tumors 24 hours after treatment with PSMA7 siRNA and RAN siRNA, 40% and 30% reduction relative to nontargeting control siRNA, respectively ($P < 0.05$, Figure 5A).

HT-29 tumors treated with PSMA7 siRNA or RAN siRNA were investigated for apoptotic activity. Three days after siRNA treatment, we performed TUNEL staining which detects apoptotic DNA breaks *in situ*. TUNEL staining of tumor tissue treated with PSMA7 siRNA and RAN siRNA revealed a significant number of apoptotic cells relative to the number in the nontargeting control siRNA treated tumors

Table 3 Correlation of *PSMA7* and *RAN* expression with liver and lung metastases in human colorectal cancer

	No of subjects	*PSMA7*		*RAN*	
	($n = 191$)	expression	*P*-value	expression	*P*-value
Liver metastasis					
Positive	41	1.108 ± 0.116	0.0762	0.597 ± 0.052	0.9112
Negative	150	0.884 ± 0.043		0.605 ± 0.031	
Lung metastasis					
Positive	29	0.870 ± 0.112	0.5336	0.460 ± 0.064	0.0233
Negative	162	0.943 ± 0.045		0.629 ± 0.029	

Note: Values are mean ± standard error.

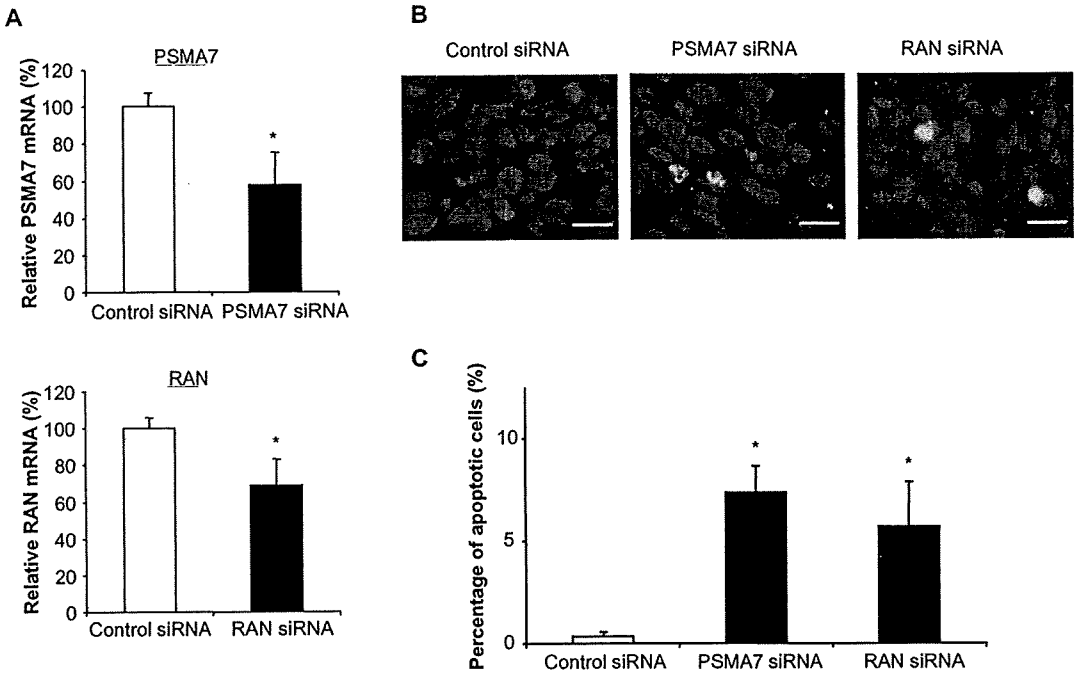

Figure 5 Apoptosis induction by PSMA7 siRNA and RAN siRNA treatment *in vivo*. **A)** Expression of PSMA7 mRNA and RAN mRNA in HT-29 tumors treated with siRNA. ($n = 4$ per group, $^*P < 0.05$). **B)** TUNEL staining of HT-29 tumor tissues treated with siRNA. Scale bar, 20 μm. **C)** TUNEL-positive cells were counted and represented ($n = 3$ per group, $^*P < 0.05$). As a control, nontargeting siRNA was used. Values are mean ± SD.
Abbreviations: PSMA7, proteasome subunit, α-type, 7; RAN, ras-related nuclear protein; SD, standard deviation; siRNA, small interfering RNAs.

($P < 0.05$, Figures 5B, 5C). These results indicate that PSMA7 siRNA and RAN siRNA induce apoptotic cell death *in vivo*.

Discussion

Molecular targeted therapy is one of the most promising approaches in cancer treatment. For cancer researchers it is now possible to understand the molecular mechanisms of the development and progression in many types of cancer. It is expected that many potential new molecular targets will be discovered for cancer therapy. To identify molecular targets for colorectal cancer therapy, we performed a sophisticated strategy using RNAi-based reverse genetics *in vitro* and *in vivo*. RNAi is a cellular mechanism for silencing of gene expression. Following the demonstration of RNAi mediated by siRNA in mammalian cells in 2001,[22] RNAi has provided new powerful tools for biological research and drug discovery. Additionally, therapeutics based on RNAi offers a new class of pharmaceutical drugs. The inhibition of gene expression through RNAi is applicable to all classes of molecular targets, including the "undruggable targets" of traditional pharmaceutical drugs such as small molecule and protein.

First, we carried out a gene expression profiling of subjects with colorectal tumors and selected 97 genes whose expression was elevated in human colorectal cancer tissues as a screening source of molecular targets. This starting from human disease samples has a great advantage, because cultured cells and disease models cannot faithfully reproduce the pathology of cancer. We then analyzed the function of genes using RNAi *in vitro* and *in vivo*. We performed a functional screening of genes by a reverse transfection-based cell transfection array to obtain an unbiased evaluation on the efficacy of a specific siRNA related to apoptosis induction in human colorectal cancer. An unbiased evaluation is important in the discovery of a new and unique target that brings a novel concept of targeted therapy. Our results showed that the siRNA designed for PSMA7 and RAN significantly promoted apoptosis of HT-29 human colon cancer cells. In our next step, we demonstrated *in vivo* proof-of-concept by the administration of siRNA to a colon tumor model. The *in vivo* delivery of PSMA7 siRNA and RAN siRNA markedly induced apoptosis in HT-29 tumors in mice. Finally, we identified PSMA7 and RAN as new molecular targets for an RNAi-based colorectal cancer therapy.

PSMA7 (also known as XAPC7) is a proteasome subunit.[23] The 26S proteasome consist of a 20S proteasome core and two 19S regulatory subunits.[24] The 20S proteasome core

is a barrel-shaped structure arranged in four stacked rings. Of these four rings, two end rings are composed of seven α-subunits, and two central rings are composed of seven β-subunits. PSMA7 is one of the seven proteasome α-subunits of 20S proteasome. PSMA7 interacts specifically with hepatitis B virus X protein (HBX), which is important in the life cycle of the hepatitis B virus (HBV).[25] In addition, PSMA7 has a principal role in regulating activity of the hepatitis C virus (HCV) internal ribosome entry site (IRES), a function essential for HCV replication.[26]

The ubiquitin–proteasome pathway is the main extra-lysosomal system involved in intracellular proteolysis and is critical for the proliferation and survival of all cells.[24,27] In particular cancerous cells, the ubiquitin-proteasome pathway plays an integral role in the mechanisms underlying carcinogenesis and metastasis, including cell cycle regulation, apoptosis, and angiogenesis.[24,27] The cancer cells exploit the proteasome for their own proliferation through the cell cycle by degrading of cell cycle regulatory proteins. Furthermore, the proteasome regulates apoptotic activity via effects on the pro-oncogenic nuclear factor (NF)-κB pathway, which is a transcriptional activator and activated in many types of tumor.[28] Under normal conditions, NF-κB is bound to its inhibitor IκB (IκB) and in an inactive state. The proteasome degrades IκB in response to cellular stresses, and then NF-κB activates transcription of genes for growth factors and apoptosis inhibitors.[24,29,30] Therefore, proteasome is an attractive target for cancer therapy. A dipeptidyl boronic acid proteasome inhibitor, bortezomib, suppresses degradation of IκB by proteasome and blocks NF-kB signaling with resultant apoptosis.[24,27,29] The efficacy of bortezomib is investigated in various types of malignancies including advanced colorectal cancer.[24,31,32] However, the ubiquitin-proteasome pathway is essential for maintenance of cell function in all cells, and the proteasome inhibitor may attack normal cells and cause severe side effects in patients.[33,34] A proteasome inhibitor specific for cancer cells should provide a better treatment with minimal side effects. In this study, among proteasome subunits genes, *PSMA7* is the only gene listed for genes whose expression is elevated in human colorectal cancer tissues. RNAi-mediated specific inhibition of PSMA7 may be a smart colorectal cancer therapy. Although it is impossible at the moment to judge whether PSMA7 silencing inhibited degradation of IκB by proteasome and blocks NF-kB signaling, in fact, our results indicated that PSMA7 siRNA caused apoptosis in HT-29 colon cells and HT-29 tumor tissues. PSMA7 was overexpressed in not only colon tumor tissues but also in other tumor tissues, which suggests that PSMA7 might be a potential target against various types of cancer.

Moreover, PSMA7 is interesting because of the correlation between its expression and the liver metastasis of colorectal cancer. Our study showed that expression of PSMA7 mRNA was elevated in colorectal tumor tissues from subjects with liver metastasis, although no statistical significance was found. Another research group also reported that overexpression of PSMA7 protein associates with liver metastasis in colorectal cancer.[35] PSMA7 may be a predictive marker and a molecular target for liver metastasis from colorectal cancer. Further investigations are needed to confirm the relationship between PSMA7 and colorectal cancer liver metastasis by gene expression profiling on a validation set of colorectal cancer subjects and analysis of PSMA7 expression on a colorectal cancer liver metastatic site at both the mRNA and protein levels.

RAN protein (Ran) is a small GTPase belonging to the Ras superfamily. Ran is essential for the translocation of RNA and proteins through the nuclear pore complex.[36,37] GTPase Ran regulates numerous cellular processes by switching between a GTP-bound and GDP-bound form.[38] Ran is also critical for the regulation of the cell cycle through mitotic spindle assembly and post-mitotic nuclear envelope assembly.[38,39]

It is reported that Ran is a suppressor of Bcl-2-associated X protein (Bax), a pro-apoptotic member of the Bcl-2 family of proteins, and that it inhibits apoptosis induced by the anticancer drug paclitaxel.[40] Furthermore, it is indicated that silencing of Ran in various tumor cell types causes aberrant mitotic spindle formation, mitochondrial dysfunction, and apoptosis.[41,42] Ran is abundantly expressed in most cancer cell lines and cancer tissues.[41] This suggests that Ran is associated with malignant transformation and/or the enhanced proliferation of cancer cells. There is a current finding that most tumor cells, but not normal tissues, become dependent on Ran signaling for cell mitosis.[41] Targeting the Ran signaling pathway may provide a selective anticancer strategy.

This study showed that RAN mRNA was elevated in colon cancer cell lines and tissues, and in some types of tumor tissue. *RAN* silencing using RAN siRNA induced apoptosis in HT-29 colon cancer cells and HT-29 tumor tissues. RAN siRNA can specifically inhibit Ran which is a main molecule of *RAN* signaling, and may be a selective inhibitor against colon cancer.

We identified PSMA7 and RAN as new molecular targets for colorectal cancer therapy using RNAi-based

screening *in vitro* and *in vivo*. In a further study, we are investigating the antitumor activity of PSMA7 siRNA and RAN siRNA in a colon cancer model and a colon cancer liver metastasis model. Induction of apoptosis is one of the main targets for cancer therapy. The inhibitors of PSMA7 and RAN may provide unique anticancer strategies based on novel mechanisms of action. Since the inhibition of gene expression through RNAi is highly specific and applicable to "undruggable targets", RNAi-based therapeutics using PSMA7 siRNA and RAN siRNA is a particularly promising approach for cancer treatment.

Acknowledgments

We thank Ms Ayako Inoue for her excellent technical assistances. This work was supported in part by a Grant-in-Aid for the Third-Term Comprehensive 10-Year Strategy for Cancer Control of Japan; a Grant-in-Aid for Scientific Research on Priority Areas Cancer from the Ministry of Education, Culture, Sports, Science and Technology, and the Program for Promotion of Fundamental Studies in Health Sciences of the National Institute of Biomedical Innovation (NiBio) of Japan. The authors report no conflicts of interest in this work.

References

1. Garcia M, Jemal A, Ward EM, et al. *Global Cancer Facts and Figures 2007*. Atlanta, GA: American Cancer Society, 2007. p. 12–14.
2. National Cancer Center. Tokyo, Japan. Cancer statistics in Japan (2008). Available from http://ganjoho.ncc.go.jp/public/statistics/backnumber/2008_en.html. Accessed July 2, 2009.
3. Hanahan D, Weinberg RA. The hallmarks of cancer. *Cell*. 2000; 100(1):57–70.
4. Baranda J, Williamson S. The new paradigm in the treatment of colorectal cancer: are we hitting the right target? *Expert Opin Investig Drugs*. 2007;16(3):311–324.
5. Köhne CH, Lenz HJ. Chemotherapy with targeted agents for the treatment of metastatic colorectal cancer. *Oncologist*. 2009;14(5):478–488.
6. Ferrara N, Kerbel RS. Angiogenesis as a therapeutic target. *Nature*. 2005;438(7070):967–974.
7. Kim KJ, Li B, Winer J, et al. Inhibition of vascular endothelial growth factor-induced angiogenesis suppresses tumour growth *in vivo*. *Nature*. 1993;362(6423):841–844.
8. Hurwitz H, Fehrenbacher L, Novotny W, et al. Bevacizumab plus irinotecan, fluorouracil, and leucovorin for metastatic colorectal cancer. *N Engl J Med*. 2004;350(23):2335–2342.
9. Wood JM, Bold G, Buchdunger E, et al. PTK787/ZK 222584, a novel and potent inhibitor of vascular endothelial growth factor receptor tyrosine kinases, impairs vascular endothelial growth factor-induced responses and tumor growth after oral administration. *Cancer Res*. 2000;60(8):2178–2189.
10. Drevs J, Hofmann I, Hugenschmidt H, et al. Effects of PTK787/ZK 222584, a specific inhibitor of vascular endothelial growth factor receptor tyrosine kinases, on primary tumor, metastasis, vessel density, and blood flow in a murine renal cell carcinoma model. *Cancer Res*. 2000;60(17):4819–4824.
11. Mellinghoff I. Why do cancer cells become "addicted" to oncogenic epidermal growth factor receptor? *PLoS Med*. 2007;4(10):1620–1622.
12. Henson ES, Gibson SB. Surviving cell death through epidermal growth factor (EGF) signal transduction pathways: implications for cancer therapy. *Cell Signal*. 2006;18(12):2089–2097.
13. Cunningham D, Humblet Y, Siena S, et al. Cetuximab monotherapy and cetuximab plus irinotecan in irinotecan-refractory metastatic colorectal cancer. *N Engl J Med*. 2004;351(4):337–345.
14. Saltz L, Easley C, Kirkpatrick P. Panitumumab. *Nat Rev Drug Discov*. 2006;5(12):987–988.
15. Taylor K, Micha D, Ranson M, Dive C. Recent advances in targeting regulators of apoptosis in cancer cells for therapeutic gain. *Expert Opin Investig Drugs*. 2006;15(6):669–690.
16. Frenzel A, Grespi F, Chmelewskij W, Villunger A. Bcl2 family proteins in carcinogenesis and the treatment of cancer. *Apoptosis*. 2009;14(4):584–596.
17. Klasa RJ, Gillum AM, Klem RE, Frankel SR. Oblimersen Bcl-2 antisense: facilitating apoptosis in anticancer treatment. *Antisense Nucleic Acid Drug Dev*. 2002;12:193–213.
18. Newsom-Davis T, Prieske S, Walczak H. Is TRAIL the holy grail of cancer therapy? *Apoptosis*. 2009;14(4):607–623.
19. Marini P, Denzinger S, Schiller D, et al. Combined treatment of colorectal tumours with agonistic TRAIL receptor antibodies HGS-ETR1 and HGS-ETR2 and radiotherapy: enhanced effects *in vitro* and dose-dependent growth delay *in vivo*. *Oncogene*. 2006;25(37):5145–5154.
20. Honma K, Iwao-Koizumi K, Takeshita F, et al. RPN2 gene confers docetaxel resistance in breast cancer. *Nat Med*. 2008;14(9):939–948.
21. Komori T, Takemasa I, Yamasaki M, et al. Gene expression of colorectal cancer: preoperative genetic diagnosis using endoscopic biopsies. *Int J Oncol*. 2008;32(2):367–375.
22. Elbashir SM, Harborth J, Lendeckel W, Yalcin A, Weber K, Tuschl T. Duplexes of 21-nucleotide RNAs mediate RNA interference in cultured mammalian cells. *Nature*. 2001;411(6836):494–498.
23. Gerards WL, de Jong WW, Boelens W, Bloemendal H. Structure and assembly of the 20S proteasome. *Cell Mol Life Sci*. 1998;54(3):253–262.
24. Adams J. The development of proteasome inhibitors as anticancer drugs. *Cancer Cell*. 2004;5(5):417–421.
25. Huang J, Kwong J, Sun EC, Liang TJ. Proteasome complex as a potential cellular target of hepatitis B virus X protein. *J Virol*. 1996;70(8): 5582–5591.
26. Krüger M, Beger C, Welch PJ, Barber JR, Manns MP, Wong-Staal F. Involvement of proteasome alpha-subunit PSMA7 in hepatitis C virus internal ribosome entry site-mediated translation. *Mol Cell Biol*. 2001;21(24):8357–8364.
27. Hoeller D, Dikic I. Targeting the ubiquitin system in cancer therapy. *Nature*. 2009;458(7237):438–444.
28. Karin M. Nuclear factor-B in cancer development and progression. *Nature*. 2006;441(7092):431–436.
29. Richardson PG, Mitsiades C, Hideshima T, Anderson KC. Proteasome inhibition in the treatment of cancer. *Cell Cycle*. 2005;4(2):290–296.
30. Palombella VJ, Rando OJ, Goldberg AL, Maniatis T. The ubiquitin-proteasome pathway is required for processing the NF-kappa B1 precursor protein and the activation of NF-kappa B. *Cell*. 1994;78(5): 773–785.
31. Cusack JC Jr, Liu R, Houston M, et al. Enhanced chemosensitivity to CPT-11 with proteasome inhibitor PS-341: implications for systemic nuclear factor-kappaB inhibition. *Cancer Res*. 2001;61(9):3535–3540.
32. Pitts TM, Morrow M, Kaufman SA, Tentler JJ, Eckhardt SG. Vorinostat and bortezomib exert synergistic antiproliferative and proapoptotic effects in colon cancer cell models. *Mol Cancer Ther*. 2009;8(2):342–349.
33. Voortman J, Giaccone G. Severe reversible cardiac failure after bortezomib treatment combined with chemotherapy in a non-small cell lung cancer patient: a case report. *BMC Cancer*. 2006;6:129.
34. Perfetti V, Palladini G, Brunetti L, et al. Bortezomib-induced paralytic ileus is a potential gastrointestinal side effect of this first-in-class anticancer proteasome inhibitor. *Eur J Gastroenterol Hepatol*. 2007;19(7):599–601.
35. Hu XT, Chen W, Wang D, et al. The proteasome subunit PSMA7 located on the 20q13 amplicon is overexpressed and associated with liver metastasis in colorectal cancer. *Oncol Rep*. 2008;19(2):441–446.

36. Kuersten S, Ohno M, Mattaj IW. Nucleocytoplasmic transport: Ran, beta and beyond. *Trends Cell Biol.* 2001;11(12):497–503.
37. Pemberton LF, Paschal BM. Mechanisms of receptor-mediated nuclear import and nuclear export. *Traffic.* 2005;6(3):187–198.
38. Joseph J. Ran at a glance. *J Cell Sci.* 2006;119(Pt 17):3481–3484.
39. Hetzer M, Gruss OJ, Mattaj IW. The Ran GTPase as a marker of chromosome position in spindle formation and nuclear envelope assembly. *Nat Cell Biol.* 2002;4(7):E177–E184.
40. Woo IS, Jang HS, Eun SY, et al. Ran suppresses paclitaxel-induced apoptosis in human glioblastoma cells. *Apoptosis.* 2008;13(10):1223–1231.
41. Xia F, Lee CW, Altieri DC. Tumor cell dependence on Ran-GTP-directed mitosis. *Cancer Res.* 2008;68(6):1826–1833.
42. Morgan-Lappe SE, Tucker LA, Huang X, et al. Identification of Ras-related nuclear protein, targeting protein for xenopus kinesin-like protein 2, and stearoyl-CoA desaturase 1 as promising cancer targets from an RNAi-based screen. *Cancer Res.* 2007;67(9):4390–4398.

Ann Surg Oncol (2009) 16:1070–1071
DOI 10.1245/s10434-008-0306-3

Annals of
SURGICAL ONCOLOGY
OFFICIAL JOURNAL OF THE SOCIETY OF SURGICAL ONCOLOGY

LETTER TO THE EDITOR

Important Matters to Identify Robust Markers for Metastasis and Recurrence in Solid Cancer

IN REPLY

We appreciate the interest of Prof. Liakakos and colleague in our article on the importance of the identification of robust genetic markers and targets to predict solid-cancer metastasis and recurrence.

Liakakos et al. describe two prospective randomized trials which concluded that locoregional control plus extended surgical lymphadenectomy and adjuvant chemotherapy significantly improved clinical outcome in the treatment of stages II and III gastric cancer.[1,2] However, in spite of the significant efforts that have been made, peritoneal recurrence as well as distant metastasis remain major problems in the treatment of gastric cancer. This observation led us to conclude that there were undetectable isolated tumor cells in the circulatory system and disseminated in the bone marrow, and we could not expect further improvements in clinical outcome until these problems are overcome. Therefore, major efforts are required to identify specific biomarkers that predict recurrence and metastasis. With regard to potentially curative treatments for gastric cancer, Liakakos et al. suggested that it was important to be able to predict the risk of distant and peritoneal dissemination, and also to identify novel therapeutic targets for the prevention of dissemination and recurrence. They also stated that, considering the number of steps required for solid-tumor metastasis, multiple markers (rather than a single marker) would be preferable. Ideally, markers should also be tailored for each patient.

We completely agree with the points they made. However, we would like to point out that, from a practical viewpoint, new markers must reside in patients' serum because circulating markers offer convenience and reduce the cost of testing. We also emphasize the report of Grey et al., who found that cells disseminate very early and evolve to metastatic disease independent from the primary tumor.[3] Thus, we must identify markers at the earliest possible phase of solid-tumor development.

With regard to finding a maker which reliably and specifically predicts metastasis and recurrence, we should reconsider the classical pathway of metastasis. Several recent studies identified multiple factors which contribute to metastasis and recurrence, as shown in Table 1. As for tumor-specific factors in Table 1, we examined markers indicating the presence of isolated tumor cells, such as circulating tumor cells and disseminated tumor cells to clarify the clinical significance of their expression.[4–8] However, we found that presence of isolated tumor cells did not accurately predict metastasis.[4] Thus, we focused on identifying cancer stem cells in solid tumors and determining whether cancer stem cells have the capacity for metastasis.[9,10] It is possible that the presence of cell surface markers in the circulatory system which are characteristic of cancer stem cells may accurately predict metastasis or recurrence. Moreover, the predictive markers for angiogenesis or invasion [vascular endothelial growth factor (VEGF), matrix metalloproteinases (MMPs)] may well be indicators for metastasis. In fact, membrane type 1 (MT1)-MMP appears to be the best marker to predict distant metastasis compared with other MMP family members.[11] Furthermore, a recent study focused on the epithelial mesenchymal transition (EMT) as a critical event leading to metastasis and the avoidance of apoptosis in peripheral blood and bone marrow.[12]

Note that metastasis and tumor recurrence also require host side cells and factors (Table 1). After receiving signals from primary cancer cells, recruitment of hematopoietic progenitor cells from bone marrow or endothelial progenitor cells in peripheral blood was observed in premetastatic niches.[13,14] Then, isolated tumor cells from primary cancers actively moved toward sites of premetastatic niche with chemokine production, thereby leading to metastasis.[15] Therefore, cell surface markers indicative of immature host cells, chemokines, and their receptors may predict metastasis and recurrence. Hougton et al. demonstrated that chronic inflammation in the gastric mucosa recruited bone-marrow-derived progenitor cells for tissue repair.[16] Therefore, we must identify both malignant cell-specific markers as well as niches and specific signals fostering metastasis.

Finally, we should focus on the presence of microRNA, which can mainly transactivate or inhibit proteins classified into both the cancer-cell-side as well as the host-side factors (Table 1).[17] Therefore, further studies will be required

TABLE 1 Aspects of the metastatic cascade

Tumor-specific factors	Host-side factors		
	Cellular factors	Local or systemic signals	Circumstances
Disseminating cancer cells	Osteoblastic niche	Chemokines	Microenvironmental niches
Circulating cancer cells	Vascular niche	Cytokines	Hypoxia
Cancer stem cells			pH
Induction of angiogenesis	Hematopoietic progenitor cells		Inflammation
Induction of lymphangiogenesis	Endothelial progenitor cells		
Metastatic (invading) ability	Mesenchymal cells		
Epithelial mesenchymal transition			
MicroRNA			

to search for the combination between miR and its regulating genes to predict clinical magnitude in bone marrow (BM) and peripheral blood (PB) from solid-cancer cases.

In conclusion, we believe that it is imperative that future studies identify biomarkers pertinent to the prevention and treatment of recurrence or metastasis of solid cancers. If both cancer-side and host-side factors are considered simultaneously, it should be possible to improve clinical outcome.

Koshi Mimori, MD, PhD, Masaaki Iwatsuki, MD
Takehiko Yokobori, MD, and Masaki Mori, PhD
Department of Surgical Oncology, Medical Institute of Bioregulation, Kyushu University, Beppu, Japan
e-mail: kmimori@beppu.kyushu-u.ac.jp

Published Online: 24 January 2009

REFERENCES

1. Sakuramoto S, Sasako M, Yamaguchi T, Kinoshita T, Fujii M, Nashimoto A, et al. Adjuvant chemotherapy for gastric cancer with S-1, an oral fluoropyrimidine. *N Engl J Med.* 2007;357:1810–20.
2. Sasako M, Sano T, Yamamoto S, Kurokawa Y, Nashimoto A, Kurita A, et al. D2 lymphadenectomy alone or with para-aortic nodal dissection for gastric cancer. *N Engl J Med.* 2008;359:453–62.
3. Gray JW. Evidence emerges for early metastasis and parallel evolution of primary and metastatic tumors. *Cancer Cell.* 2003;4:4–6.
4. Mimori K, Fukagawa T, Kosaka Y, Kita Y, Ishikawa K, Etoh T, et al. Hematogenous metastasis in gastric cancer requires isolated tumor cells and expression of vascular endothelial growth factor receptor-1. *Clin Cancer Res.* 2008;14:2609–16.
5. Mori M, Mimori K, Inoue H, Barnard GF, Tsuji K, Nanbara S, et al. Detection of cancer micrometastases in lymph nodes by reverse transcriptase-polymerase chain reaction. *Cancer Res.* 1995;55:3417–20.
6. Mori M, Mimori K, Tanaka F, Ueo H, Sugimachi K, Akiyoshi T. Molecular diagnosis of circulating cancer cells using MAGE gene assays. *JAMA.* 1997;278:476–7.
7. Mori M, Mimori K, Ueo H, Karimine N, Barnard GF, Sugimachi K, et al. Molecular detection of circulating solid carcinoma cells in the peripheral blood: the concept of early systemic disease. *Int J Cancer.* 1996;68:739–43.
8. Mori M, Mimori K, Ueo H, Tsuji K, Shiraishi T, Barnard GF, et al. Clinical significance of molecular detection of carcinoma cells in lymph nodes and peripheral blood by reverse transcription-polymerase chain reaction in patients with gastrointestinal or breast carcinomas. *J Clin Oncol.* 1998;16:128–32.
9. Haraguchi N, Ohkuma M, Sakashita H, Matsuzaki S, Tanaka F, Mimori K, et al. CD133+CD44+ population efficiently enriches colon cancer initiating cells. *Ann Surg Oncol.* 2008;15:2927–33.
10. Haraguchi N, Utsunomiya T, Inoue H, Tanaka F, Mimori K, Barnard GF, et al. Characterization of a side population of cancer cells from human gastrointestinal system. *Stem Cells.* 2006;24:506–13.
11. Mimori K, Fukagawa T, Kosaka Y, Ishikawa K, Iwatsuki M, Yokobori T, et al. A large-scale study of MT1-MMP as a marker for isolated tumor cells in peripheral blood and bone marrow in gastric cancer cases. *Ann Surg Oncol.* 2008;15:2934–42.
12. Karnoub AE, Dash AB, Vo AP, Sullivan A, Brooks MW, Bell GW, et al. Mesenchymal stem cells within tumour stroma promote breast cancer metastasis. *Nature.* 2007;449:557–63.
13. Kaplan RN, Riba RD, Zacharoulis S, Bramley AH, Vincent L, Costa C, et al. VEGFR1-positive haematopoietic bone marrow progenitors initiate the pre-metastatic niche. *Nature.* 2005;438:820–7.
14. Lyden D, Hattori K, Dias S, Costa C, Blaikie P, Butros L, et al. Impaired recruitment of bone-marrow-derived endothelial and hematopoietic precursor cells blocks tumor angiogenesis and growth. *Nat Med.* 2001;7:1194–201.
15. Avecilla ST, Hattori K, Heissig B, Tejada R, Liao F, Shido K, et al. Chemokine-mediated interaction of hematopoietic progenitors with the bone marrow vascular niche is required for thrombopoiesis. *Nat Med.* 2004;10:64–71.
16. Houghton J, Stoicov C, Nomura S, Rogers AB, Carlson J, Li H, et al. Gastric cancer originating from bone marrow-derived cells. *Science.* 2004;306:1568–71.
17. Calin GA, Ferracin M, Cimmino A, Di Leva G, Shimizu M, Wojcik SE, et al. A MicroRNA signature associated with prognosis and progression in chronic lymphocytic leukemia. *NEngl J Med.* 2005;353:1793–801.

STEM CELLS®
TISSUE-SPECIFIC STEM CELLS

Roundabout 4 Is Expressed on Hematopoietic Stem Cells and Potentially Involved in the Niche-Mediated Regulation of the Side Population Phenotype

FUMI SHIBATA,[a] YUKO GOTO-KOSHINO,[a] YOSHIHIRO MORIKAWA,[b] TADASUKE KOMORI,[b] MIYUKI ITO,[c] YUMI FUKUCHI,[c] JEFFREY P. HOUCHINS,[d] MONICA TSANG,[d] DEAN Y. LI,[e,f] TOSHIO KITAMURA,[a] HIDEAKI NAKAJIMA[c]

[a]Division of Cellular Therapy, Advanced Clinical Research Center, and [c]Center of Excellence, Institute of Medical Science, University of Tokyo, Tokyo, Japan; [b]Department of Anatomy and Neurobiology, Wakayama Medical College, Wakayama, Japan; [d]R&D Systems Inc., Minneapolis, Minnesota, USA; Departments of [e]Oncological Sciences and [f]Medicine, University of Utah, Salt Lake City, Utah, USA

Key Words. Hematopoietic stem cell • Robo • Roundabout • Slit • Surface marker

ABSTRACT

Roundabout (Robo) family proteins are immunoglobulin-type cell surface receptors that are expressed predominantly in the nervous system. The fourth member of this family, Robo4, is distinct from the other family members in that it is expressed specifically in endothelial cells. In this study, we examined the expression of Robo4 in hematopoietic stem cells (HSCs) and its possible role in HSC regulation. Robo4 mRNA was specifically expressed in murine HSCs and the immature progenitor cell fraction but not in lineage-positive cells or differentiated progenitors. Moreover, flow cytometry showed a correlation between higher expression of Robo4 and immature phenotypes of hematopoietic cells. Robo4^{high} hematopoietic stem/progenitor cells presented higher clonogenic activity or long-term repopulating activity by colony assays or transplantation assays, respectively. A ligand for Robo4, Slit2, is specifically expressed in bone marrow stromal cells, and its expression was induced in osteoblasts in response to myelosuppressive stress. Interestingly, overexpression of Robo4 or Slit2 in HSCs resulted in their decreased residence in the c-Kit$^+$Sca-1$^+$Lineage$^-$-side population fraction. These results indicate that Robo4 is expressed in HSCs, and Robo4/Slit2 signaling may play a role in HSC homeostasis in the bone marrow niche. STEM CELLS *2009;27:183–190*

Disclosure of potential conflicts of interest is found at the end of this article.

INTRODUCTION

Roundabout (Robo) family proteins are immunoglobulin-type cell surface receptors that are expressed predominantly in the nervous system [1]. Slit, a ligand for Robo, is a large secreted protein that is also expressed in brain [1]. The Robo family comprises four family members, Robo1–Robo4, and the Slit family consists of three family members, Slit1–Slit3. Robo and Slit were first described in *Drosophila* as critical molecules in axon path finding and migration of neuronal cells [2]. In mammals, Slit/Robo signaling acts as a repulsive axon guidance cue for developing neurons and inhibits neuronal migration, thus playing a critical role for correct wiring of the neuronal network [3]. In the hematopoietic system, Slit2 has been shown to inhibit chemotactic migration of lymphocytes induced by SDF-1 [4]. In addition, Slit2/Robo1 signaling plays a critical role in tumor angiogenesis [5]. Robo4 was first identified by in silico database mining as a homolog of Robo1 [6, 7]. Robo4 is unique in its expression pattern that is specific to endothelial cells, whereas it shows functional similarity to other Robo family members, such as a binding with Slit2 or an inhibitory effect for cellular migration [7]. In hematopoiesis, Forsberg et al. have reported an extensive transcriptome analysis of long-term (LT)-hematopoietic stem cells (HSCs), short-term (ST)-HSCs, and multipotent progenitors (MPPs) and showed that Robo4 is one of the differentially expressed genes among these three primitive hematopoietic cell populations [8]. However, differential expression of Robo4 in whole hematopoietic system has not been examined.

HSCs are a rare population of cells that can support life-long hematopoiesis. They are characterized by their unique capacity to self-renew and differentiate into all blood cell lineages. HSCs reside in the specific microenvironment known as the niche in the adult bone marrow (BM). The niche is thought to be located on the surface of trabecular bones, and osteoblasts lining the surface of these bones are reported to be one of the critical niche components [9, 10]. Side population (SP) phenotype, identified by as the activity of Hoechst 33342 dye efflux, is one of the hallmarks of

Author contributions: F.S., Y.G.-K., Y.M., T.K., M.I., and Y.F.: Collection and assembly of data; J.P.H., M.T., and D.Y.L.: provision of study material; T.K.: administrative support; H.N.: conception and design, financial support, data analysis and interpretation, manuscript writing, final approval of manuscript. F.S. and Y.G.-K. contributed equally to this work.

Correspondence: Hideaki Nakajima, M.D., Ph.D., Division of Hematology, Department of Internal Medicine, Keio University School of Medicine, 35 Shinanomachi, Shinjuku-ku, Tokyo 160-8582, Japan. Telephone: 81-3-5363-3785; Fax: 81-3-3353-3515; e-mail: hnakajim@sc.itc.keio.ac.jp Received April 4, 2008; accepted for publication September 30, 2008; first published online in STEM CELLS *EXPRESS* October 16, 2008. ©AlphaMed Press 1066-5099/2008/$30.00/0 doi: 10.1634/stemcells.2008-0292

quiescent HSCs in the BM niche [11, 12]. It has been shown that many of the quiescent HSCs reside in the c-Kit$^+$Sca-1$^+$Lineage$^-$ (KSL)-SP, and angiopoietin-1/Tie-2 signaling induces HSC quiescence and increases cells in the KSL-SP [13]. Moreover, quiescent HSCs move from the SP to a main population (MP) of non-SP cells when they are recruited into the cell cycle upon myelosuppressive stimuli, such as 5-fluorouracil (5-FU) treatment. However, the molecular mechanism regulating this transition remains unclear.

In a search for novel surface molecules expressed on HSCs, we found that Robo4 was highly expressed in the HSCs and the immature progenitor cell fraction. Moreover, Slit2 was specifically expressed in bone marrow stromal cells, and interestingly, the expression was induced in osteoblasts in response to myelosuppressive stimuli, such as 5-FU treatment. Surprisingly, enhanced Slit2/Robo4 signaling in HSCs resulted in the shift of their residence from SP to non-SP. These results suggest a possible involvement of Slit2/Robo4 signaling in the regulation of HSC homeostasis by the BM niche.

Materials and Methods

Cells and Mice

MS10, PA6, and OP9 cells [14, 15] were cultured as previously described [16]. Primary BM stromal cells were obtained by culturing the adherent fraction of whole BM cells from B6 mice in α-minimal essential medium/10% fetal bovine serum on the culture dish and expanding them for 2 weeks.

RNA Extraction and Reverse Transcription-Polymerase Chain Reaction

Messenger RNA (mRNA) was isolated using a Micro-FastTrack 2.0 mRNA Isolation Kit (Invitrogen, Carlsbad, CA, http://www.invitrogen.com) according to the manufacturer's protocol. First-strand cDNA was synthesized with SuperScript II reverse transcriptase (Invitrogen). The quantity of cDNA was normalized according to the expression of glyceraldehyde-3-phosphate dehydrogenase measured by real-time reverse transcription (RT)-polymerase chain reaction (PCR) using a Light Cycler Fast Start DNA SYBR Green I kit (Roche Diagnostics, Basel, Switzerland, http://www.roche-applied-science.com). Semiquantitative RT-PCR was performed using Ex Taq-HS polymerase (Takara Bio, Shiga, Japan, http://www.takara-bio.com). The sequences of primers used for RT-PCR are shown in supporting information Table 1.

Antibodies

Anti-mouse c-Kit-allophycocyanin (APC) (2B8), Sca-1-fluorescein isothiocyanate (FITC) (D7), Sca-1-APC (D7), and CD34-FITC (RAM34) antibodies were from BD Pharmingen (San Diego, http://www.bdbiosciences.com/index_us.shtml). Anti-mouse c-Kit-phycoerythrin (PE)-Cy7 (2B8) was from BioLegend (San Diego, http://www.biolegend.com). Anti-mouse Robo4 monoclonal antibodies were raised against the extracellular domain of Robo4 by immunizing rats with Y3Ag1.2.3 cells expressing mouse Robo4. The purified antibodies were labeled with PE using PhycoLink R-Phycoerythrin Conjugation Kit (PROzyme, San Leandro, CA, http://www.prozyme.com).

Flow Cytometry

BM cells were obtained by flushing out femurs and tibias from 8–12-week-old mice with phosphate-buffered saline (PBS). Depletion of lineage-positive cells and staining and fluorescence-activated cell sorting (FACS) of KSL and CD34$^-$KSL cells were described previously [17]. Stained cells were analyzed by FACSAria or FACSVantage (Becton, Dickinson and Company, Franklin Lakes, NJ, http://www.bd.com). Hoechst staining of lineage depleted cells was performed with 5 μg/ml Hoechst 33342 (Sigma-Aldrich, St. Louis, http://www.sigmaaldrich.com)

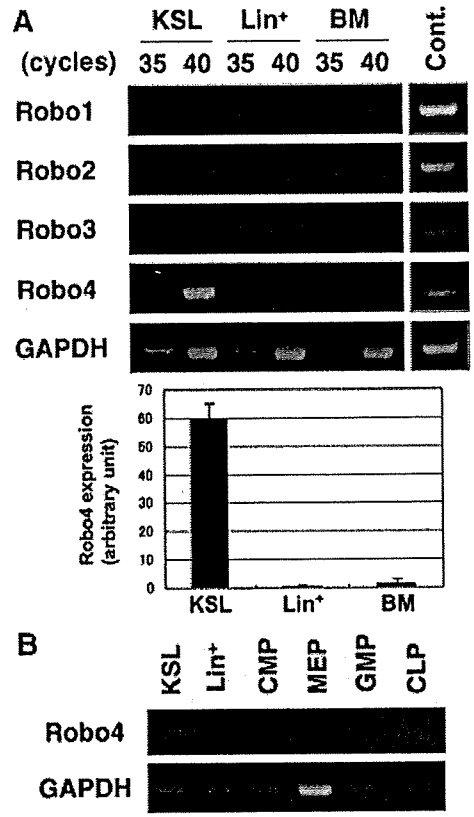

Figure 1. Expression of Robo4 in primitive hematopoietic cells. **(A):** Expression of Robo family genes. KSL and Lin$^+$ cells were sorted by flow cytometry and subjected to RNA extraction. Upper panel: the expressions of the Robo1–Robo4 genes were examined by reverse transcription (RT)-polymerase chain reaction (PCR). The GAPDH gene was examined as a cont. Brain cDNA was used as a positive cont. Lower panel: quantitative RT-PCR for the Robo4 gene (mean ± SD; $n = 3$). **(B):** The expression of the Robo4 gene in various hematopoietic progenitors was examined by RT-PCR. Abbreviations: BM, bone marrow; CLP, common lymphoid progenitor; CMP, common myeloid progenitor; Cont., control; GAPDH, glyceraldehyde-3-phosphate dehydrogenase; GMP, granulocyte/monocyte progenitor; KSL, c-Kit$^+$Sca-1$^+$Lineage$^-$; Lin, lineage marker; MEP, megakaryocyte/erythroid progenitor; Robo, roundabout.

at 37°C for 90 minutes as previously described by Goodell et al. [11].

Retrovirus Production, Infection, and Bone Marrow Transplantation

Retrovirus was produced as previously described [16]. Briefly, retrovirus plasmids [18] were transiently transfected into PLAT-E [19] cells using Fugene (Roche Diagnostics), and retrovirus supernatant was collected after 48 hours of transfection. Infection of BM cells with retrovirus was carried out using Retronectin (Takara Bio) according to the manufacturer's protocol. Bone marrow transplantation of infected cells was performed as previously described [16] using B6-Ly5.1 mice (Sankyo Lab Service Co., Tokyo, http://www.sankyolabo.co.jp) as donors and B6-Ly5.2 mice (CLEA Japan, Tokyo, http://www.clea-japan.com) as recipients and competitors. For competitive repopulation assay of Robo4$^+$KSL or Robo4$^-$KSL cells, 100 cells for each group were sorted from BM mononuclear cells of B6-Ly5.1 mice and transplanted with 2×10^5 competitor cells (whole BM cells from Ly5.2 mice) into lethally irradiated (950R) recipient mice (B6-Ly5.2). Eight- to 12-week-old mice were used in all experiments. All animal experiments were reviewed and approved by the institutional review board of the Institute of Medical Science, University of Tokyo.

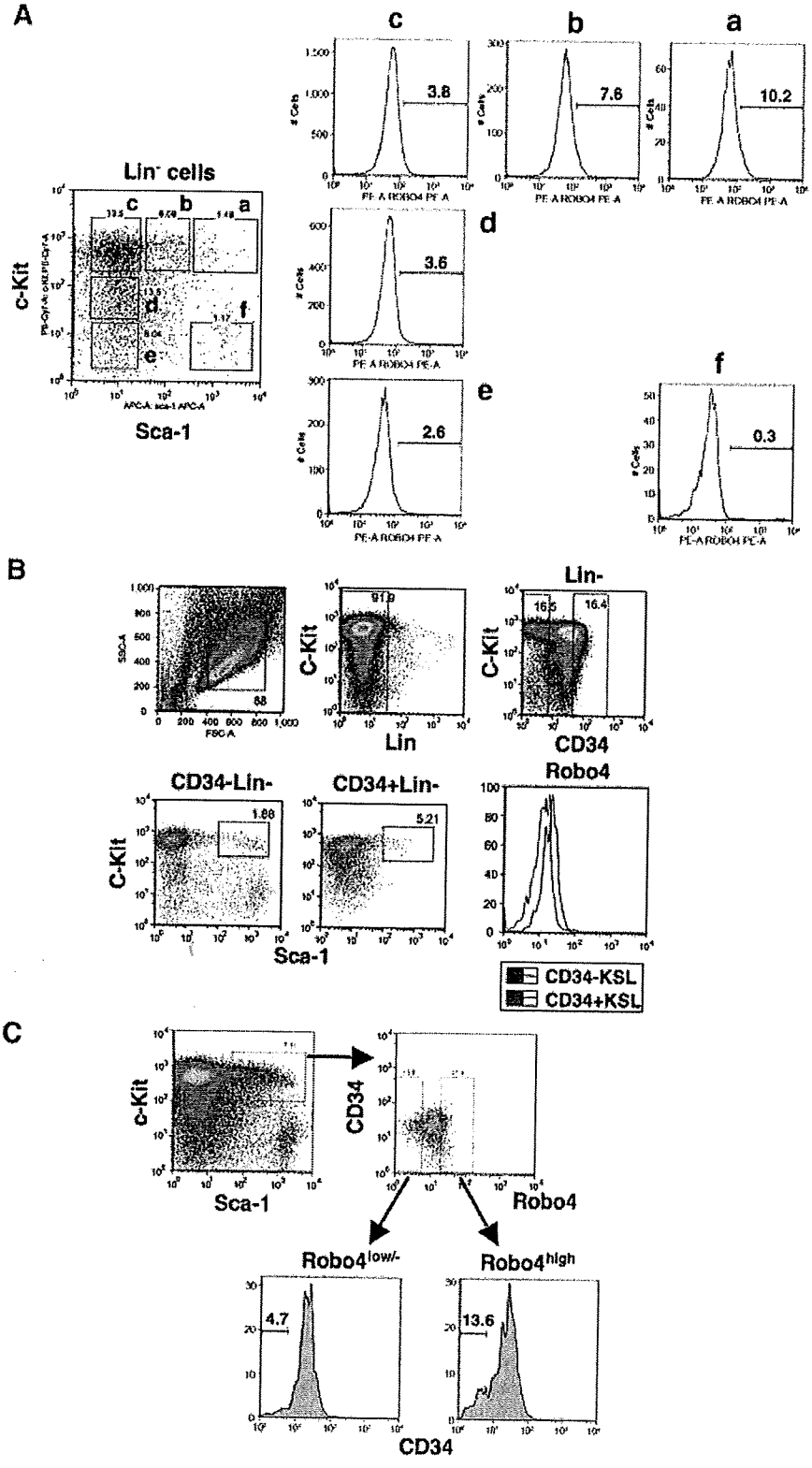

Figure 2. Expression of Robo4 by flow cytometry. **(A):** Lineage-depleted murine bone marrow cells were stained with Sca-1-fluorescein isothiocyanate (FITC), c-Kit-APC, and Robo4-PE. Cells were fractionated according to the expression of c-Kit and Sca-1 into six populations **(Aa–Af)**, and the expression of Robo4 in each fraction was analyzed. **(B):** Robo4 is highly expressed in $CD34^-KSL$ cells. $CD34^-KSL$ and $CD34^+KSL$ cells were gated as shown in the figure and examined for Robo4. **(C):** $Robo4^{high}KSL$ cells contain more $CD34^-$ cells. $Robo4^{high}KSL$ or $Robo4^{low/-}KSL$ cells were gated as shown and examined for CD34 expression. Abbreviations: FSC, forward scatter; KSL, $c\text{-}Kit^+Sca\text{-}1^+Lineage^-$; Lin, lineage marker; PE, phycoerythrin; Robo, roundabout; SSC, side scatter.

Colony-Forming Cell Assay

For the colony-forming cell assay, cells were sorted by FACS and deposited into MethoCult GF M3434 (StemCell Technologies, Vancouver, BC, Canada, http://www.stemcell.com). The number and type of colonies were assessed at day 7 of culture.

Immunostaining

Mice treated with 5-FU (150 mg/kg, i.p.) for 3 days were fixed by perfusing them with Zamboni's fixative. Femurs were then dissected and decalcified in 10% EDTA at 4°C. The bones were embedded in Tissue-Tek OCT Compound (Sakura Finetek, Tor-

rance, CA, http://www.sakura.com), frozen, and sectioned in 5-μm-thick slices using a cryostat (Leica, Heerbrugg, Switzerland, http://www.leica.com). Sections were blocked with biotin and normal donkey serum and stained with anti-Slit2 (G-19; Santa Cruz Biotechnology Inc., Santa Cruz, CA, http://www.scbt.com) and anti-osteopontin (Takara Bio) antibodies, which were then subjected to secondary staining with anti-goat IgG-biotin and anti-mouse IgG-Cy3 and tertiary staining with streptoavidin-Cy2. Sections were washed three times for 5 minutes in PBS between steps and finally mounted in Vectashield anti-fading medium (Vector Laboratories, Burlingame, CA, http://www.vectorlabs.com) containing 4,6-diamidino-2-phenylindole (Sigma-Aldrich) for nuclear labeling. Fluorescent images were examined and captured using a laser confocal microscope (Olympus, Tokyo, http://www.olympus-global.com).

Statistical Analysis

All statistical analyses were performed by unpaired Student's *t* test using GraphPad Prism software (GraphPad Software, La Jolla, CA, http://www.graphpad.com).

RESULTS

Robo4 Is Highly Expressed in Murine Hematopoietic Stem Cells and Immature Hematopoietic Progenitors

During a search for novel surface molecules expressed on HSCs, we noticed that cells in the hematopoietic and the nervous systems share a number of expressed genes [20–22]. These observations prompted us to investigate the expression of Robo family genes in the hematopoietic system. We first checked the expression of Robo family genes by RT-PCR. Interestingly, Robo4 was specifically expressed in murine KSL cells, which contain HSCs and immature hematopoietic progenitors. However, it was not expressed in lineage marker-positive (Lin^+) cells or various early hematopoietic progenitors, such as common myeloid progenitor, megakaryocyte/erythroid progenitor, granulocyte/monocyte progenitor, and common lymphoid progenitor (Fig. 1A, 1B). These data suggest that Robo4 is specifically expressed in murine HSCs and immature hematopoietic progenitors. In fact, $Robo4^+CD34^-KSL$ cells induced to differentiate in vitro no longer expressed Robo4 (supporting information Fig. 1), indicating that Robo4 is downregulated along with differentiation. Collectively, these results suggest that Robo4 is expressed in murine HSCs and immature hematopoietic progenitors, and its expression declines as the cells differentiate.

Analysis of Robo4 Expression by Flow Cytometry

We then generated a monoclonal antibody specific for Robo4 and examined its expression by flow cytometry (FACS). The antibody was specific to Robo4 (supporting information Fig. 2) and was not cross-reactive with other Robo family members (data not shown). Compatible with RT-PCR data, Robo4 was not expressed in lineage marker-positive cells in the murine BM (data not shown). As shown in Figure 2A, the highest expression of Robo4 was detected in the tip population of KSL cells (fraction a), which is enriched in HSCs. Furthermore, $CD34^-KSL$ cells, a highly enriched population of long-term HSCs, expressed higher Robo4 compared with $CD34^+KSL$ cells, an enriched fraction of short-term HSCs (Fig. 2B). Conversely, $Robo4^{high}KSL$ cells contained more $CD34^-KSL$ cells compared with $Robo4^{low/-}KSL$ cells (13.6% vs. 4.7%, respectively) (Fig. 2C). Taken together, these results confirm high expression of Robo4 in murine HSCs and immature hematopoietic progenitors.

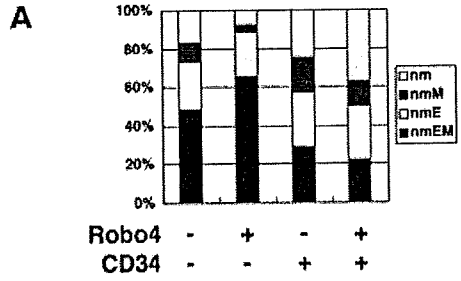

	nmEM	nmE	nmM	nm
Robo4⁻CD34⁻	48 ± 3	24 ± 3	10 ± 2	17 ± 3
Robo4⁺CD34⁻	66 ± 4 *	23 ± 2	4 ± 1	8 ± 2
Robo4⁻CD34⁺	29 ± 3 *	28 ± 4	18 ± 2	25 ± 3
Robo4⁺CD34⁺	23 ± 4	28 ± 4	13 ± 3	37 ± 5

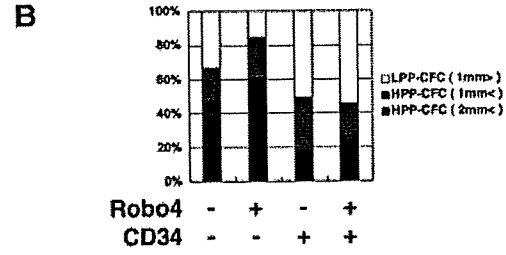

	HPP-CFC (> 2 mm)	HPP-CFC (1-2 mm)	LPP-CFC (< 1 mm)
Robo4⁻CD34⁻	47 ± 4	20 ± 2	33 ± 4
Robo4⁺CD34⁻	64 ± 5 *	21 ± 3	15 ± 2
Robo4⁻CD34⁺	19 ± 3 *	31 ± 3	51 ± 4
Robo4⁺CD34⁺	27 ± 5	19 ± 3	56 ± 3

Figure 3. Clonogenic activities of $Robo4^{high}$ hematopoietic stem/progenitor cells. **(A, B):** Murine $c\text{-}Kit^+Sca\text{-}1^+Lineage^-$ cells were clonally sorted into a 96-well dish (single cell per well) according to the expression of CD34 and Robo4 by fluorescence-activated cell sorting and subjected to clonogenic analyses. Two hundred cells were assessed for each sorted fraction, and the data are from three independent experiments. Colonies were assessed for their differentiation capacity **(A)** or colony size **(B)**. Graphs show percentage of colonies in each sorted fraction (total colony number was regarded as 100%). Tables show actual percentage of colonies (mean ± SD; $n = 3$). *, $p < .01$. $Robo4^+$ and $Robo4^-$ stand for $Robo4^{high}$ and $Robo4^{low/-}$ cells, respectively. LPP-CFCs were less than 1 mm in diameter; HPP-CFCs were more than 1 mm in diameter. Abbreviations: CFC, colony-forming cell; E, erythroid; HPP, high proliferating potential; LPP, low proliferating potential; m, macrophage; M, megakaryocyte; n, neutrophil; Robo, roundabout.

Expression of Robo4 Correlates with High Multipotentiality and Long-Term Repopulating Potential

We next examined the physiological relevance of Robo4 expression and the HSC activities. As shown in Figure 3A and 3B, $Robo4^{high}CD34^-KSL$ cells presented higher multilineage differentiation (shown as nmEM in Fig. 3A) and proliferative potential (shown as high proliferating potential-colony-forming cells in Fig. 3B) compared with other fractions. Interestingly, transplantation assays revealed that long-term repopulating activity of KSL cells was detected only in the $Robo4^{high}$ fraction and not in the $Robo4^{low/-}$ fraction (Fig. 4). These results suggest that higher expression of Robo4 defines a population of cells with higher capacities for mul-

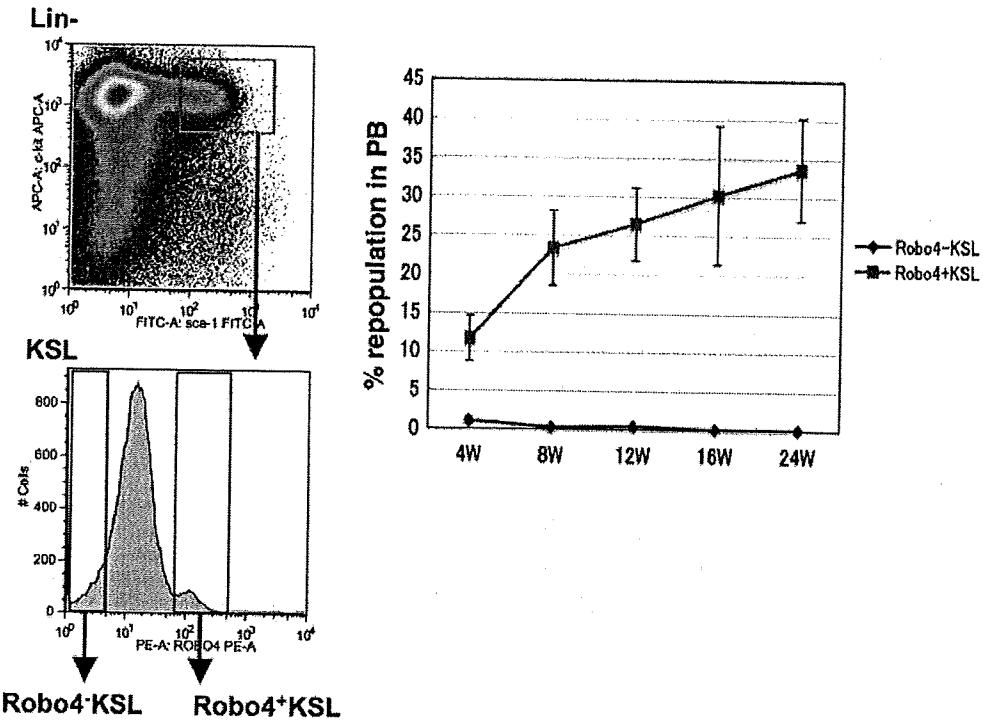

Figure 4. Long-term repopulating potential of Robo4^{high} and Robo4$^{low/-}$ hematopoietic stem/progenitor cells. KSL cells were sorted according to the expression of Robo4 and subjected to long-term repopulating assays as described in Materials and Methods. One hundred cells of each fraction were sorted and transplanted into each recipient mouse. The contribution of donor cells (percentage) in the recipients' PB was examined at the indicated time points. Data are mean ± SEM (n = 12 for each group). Representative data from three independent experiments are shown. Abbreviations: FITC, fluorescein isothiocyanate; KSL, c-Kit$^+$Sca-1$^+$Lineage$^-$; PB, peripheral blood; Robo, roundabout; W, weeks.

tilineage differentiation, proliferation, and long-term repopulation.

Slit2 Is Expressed in BM Stromal Cells and Induced in Osteoblasts by Myelosuppressive Stress

To obtain clues for the role of Robo4 in HSC regulation, we examined the expression of Slit2, a ligand for Robo4, by RT-PCR. As shown in Figure 5A, Slit family genes were not expressed in hematopoietic cells, such as KSL or Lin$^+$ cells. Interestingly, however, Slit2 was expressed in murine BM stromal cell lines (Fig. 5B) and the primary BM stromal cells (Fig. 5C). Of note, primary BM stromal cells also showed slight or moderate expression of Slit 1, Slit3, and Robo1. These results suggest that Slit2 is expressed in the BM microenvironment.

We went on to investigate the role of Slit2-Robo4 signaling in HSC physiology by examining the expression of Slit2 in the BM under a stress condition. We treated mice with a cytotoxic agent, 5-FU, and periodically monitored the expression of Slit2 in the BM by RT-PCR. Interestingly, Slit2 was transiently induced in the bone marrow on days 3–6 after 5-FU treatment, whereas Slit1 and Slit3 were not induced at all (Fig. 6A). Fractionation of BM cells by CD45 expression revealed that the induction occurred in CD45$^-$ cells, suggesting that Slit2 was induced in nonhematopoietic cells (Fig. 6B). Of note, a slight induction of Slit2 was also seen in CD45$^+$ cells after 9 days of 5-FU administration. The expression of Robo4 was also upregulated in the BM after 5-FU treatment, probably because of the concentration of immature hematopoietic cells in the BM (supporting information Fig. 3).

Given that Slit2 is induced in CD45$^-$ cells, we speculated that Slit2 might be induced in the BM niche in response to myelosuppressive stress. To test this hypothesis, we performed

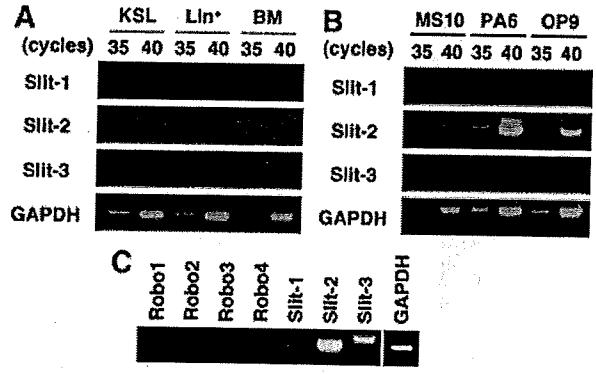

Figure 5. Expression of Slit genes in hematopoietic or BM stromal cells. **(A, B):** The expressions of Slit1–Slit3 genes were examined in KSL, Lin-positive, and whole BM cells **(A)** and various BM stromal cell lines **(B)** by reverse transcription-polymerase chain reaction (PCR). The amount of mRNA was normalized according to the expression of GAPDH. **(C):** The expression of Robo and Slit genes in primary BM stroma. Primary BM stromal cells were isolated by adherence to the culture dish, expanded, and subjected to PCR analysis. PCR was run for 40 cycles for Robo or Slit family genes and for 30 cycles for GAPDH. Abbreviations: BM, bone marrow; GAPDH, glyceraldehyde-3-phosphate dehydrogenase; KSL, c-Kit$^+$Sca-1$^+$Lineage$^-$; Lin, lineage marker; Robo, roundabout.

immunostaining of Slit2 in the BM treated with 5-FU for 3 days. As shown in Figure 6C, Slit2 was specifically induced in the osteoblasts at the endosteal surface of the bone marrow, where the HSC niche was reported to be located. Of note, expression of Slit2 was not detected in other places in the BM, such as endothelial cells (data not shown). These results suggest that

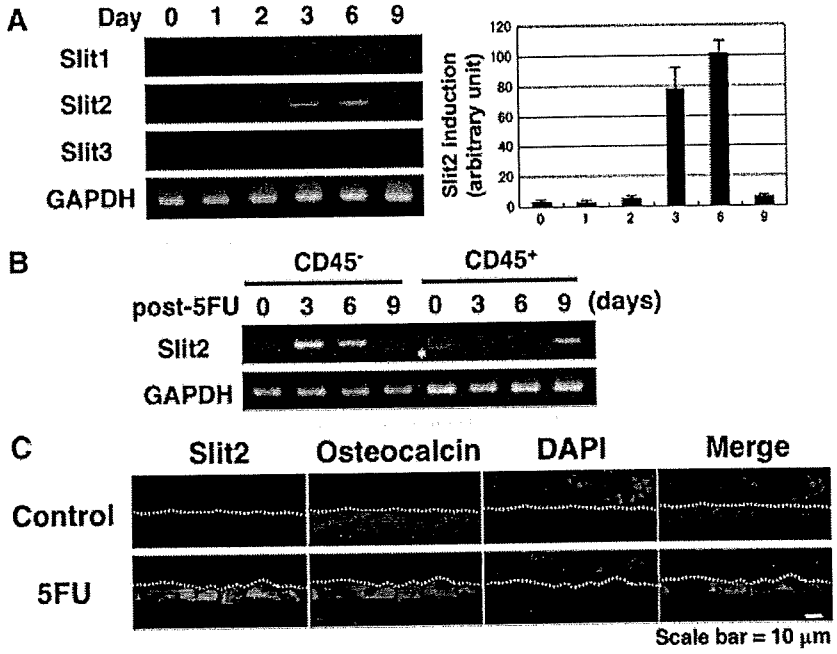

Figure 6. Induction of Slit2 in osteoblasts in response to myelosuppression. (A): Mice were treated with 5FU (150 mg/kg, i.p.), and the bone marrow (BM) cells were harvested at the indicated time points. Left panel: the expressions of Slit genes in whole BM cells were analyzed by reverse transcription (RT)-polymerase chain reaction (PCR). PCR was run for 35 cycles. Right panel: quantitative-RT-PCR for the Slit2 gene (mean ± SD; n = 3). (B): BM cells were harvested from 5FU-treated mice at the indicated time points. $CD45^+$ and $CD45^-$ cells were sorted by fluorescence-activated cell sorting and subjected to RT-PCR. PCR was run for 35 cycles. Asterisk indicates a nonspecific band. (C): Sections of femurs prepared from mice treated with 5FU for 3 days were immunostained with anti-Slit2 and osteocalcin antibodies. Nuclei were counterstained with DAPI. Broken lines indicate the margin of the bone surface. Abbreviations: DAPI, 4,6-diamidino-2-phenylindole; 5FU, 5-fluorouracil; GAPDH, glyceraldehyde-3-phosphate dehydrogenase.

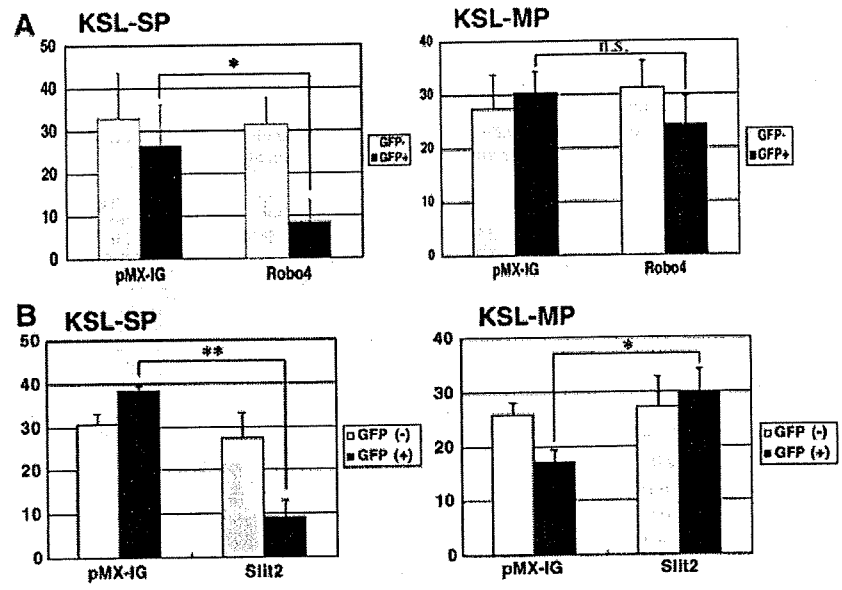

Figure 7. The role of Robo4/Slit2 signaling in SP-non-SP transition of HSCs. (A, B): Bone marrow (BM) mononuclear cells from mice treated with 5-fluorouracil (150 mg/kg, i.p.) were transduced with Robo4 (A), Slit2 (B), and mock vector (pMX-IG) by retrovirus. Equal numbers (1×10^4 cells) of infected and noninfected cells were sorted by fluorescence-activated cell sorting (FACS), mixed, and transplanted into lethally irradiated recipient mice. The BM cells were harvested after 3 months of transplantation, and the percentage of KSL-SP or KSL-MP in GFP^+ or GFP^- cells was analyzed by FACS (mean ± SD; n = 3). *, $p < .05$; **, $p < .01$. Abbreviations: GFP, green fluorescent protein; KSL, c-Kit^+Sca-$1^+$$Lineage^-$; MP, main population; n.s.; not significant by unpaired t test; Robo, roundabout; SP, side population.

Slit2-Robo4 signaling may play a role in HSC physiology in the osteoblastic niche upon myelosuppressive stress.

The Effect of Enhanced Robo4/Slit2 Signaling in SP to Non-SP Transition of HSCs

To gain more insight into the physiological role of Slit2/Robo4 signaling in HSCs, we enhanced Slit2/Robo4 signals by overexpressing Robo4 or Slit2 in the hematopoietic stem/progenitor cells and examined its effect on their SP phenotype. We retrovirally transduced Robo4 or Slit2 into the BM cells taken from 5-FU-treated mice and transplanted them into lethally irradiated recipients (Fig. 7A, 7B; supporting information Fig. 4). Robo4- or Slit2-expressing cells homed to and engrafted to the recipient's BM, albeit to a lesser extent compared with the mock control, and their contribution to the peripheral blood progressively decreased over time (supporting information Fig. 5). To our surprise, the percentage of KSL-SP was significantly lower in cells expressing Robo4 or Slit2 (green fluorescent protein $[GFP]^+$) compared with cells expressing mock vector (GFP^+) or nontransfected donor-derived cells (GFP^-) after 12 weeks of transplantation. In contrast, the percentage of KSL-MP was increased or remained constant in Slit2- or Robo4-transfected populations. On the basis of these observations, we speculated that Slit2/Robo4 signals might be acting to drive cells in KSL-SP into the KSL-MP or KSL-non-SP fraction. It is also possible that KSL-SP cells underwent apoptosis by enhanced Slit2/Robo4 signals. However, we speculate this is not the case, since we did not see any increased apoptosis in Robo4- or Slit2-overexpressing cells. In support of above hypothesis, Robo4 was highly expressed in KSL-SP cells (supporting information Fig. 6), indicating that these cells are sensitive to Slit2 stimuli. Taken together, these findings suggest that Slit2/Robo4 signaling promotes SP to non-SP transition of HSCs.

DISCUSSION

During the search for novel surface molecules expressed on primitive hematopoietic cells, we noticed that cells in the hematopoietic and nervous systems share a number of expressed genes. For example, we have previously reported that mKirre, which is abundantly expressed in brain and BM stromal cells, plays a critical role in maintaining HSC functions [20, 21]. Ephrins and their receptors, Ephs, are expressed in both the nervous and the hematopoietic systems, and they play critical roles in various aspects of neurogenesis and hematopoiesis [23–25]. Goolsby et al. also reported that hematopoietic progenitors express a set of neural genes [22]. These observations prompted us to focus on Robo family proteins, cell surface receptors that play a critical role in the nervous system. Within this family, Robo4 drew our particular attention, as the expression of Robo4 was specific to endothelial cells (ECs), and many HSC markers, such as CD34 and Flk1, were shared with ECs [26–28]. As expected, this study demonstrated that Robo4 is highly expressed in murine HSCs and immature hematopoietic progenitors. Moreover, transplantation experiments revealed that KSL cells with high Robo4 expression possessed higher long-term repopulating activity. These results demonstrate that the expression of Robo4 correlates with higher HSC capacities, such as long-term repopulation and differentiation to multiple lineages. During the course of our study, Forsberg et al. reported an extensive transcriptome analysis of LT-HSCs, ST-HSCs, and MPPs and showed that Robo4 is one of the differentially expressed genes among these three primitive hematopoietic cell populations [8]. In the current study, however, we demonstrated that the expression of Robo4 is highest in LT-HSCs not only among primitive hematopoietic cells, but also among all hematopoietic cells, including various progenitors and lineage marker-positive cells. In addition, we confirmed this observation on both the mRNA and the protein levels. Furthermore, we demonstrated that Robo4 could be used for isolating HSCs with long-term repopulating potential when combined with KSL phenotype.

Robo/Slit signaling acts as a repulsive axon guidance cue and inhibits migration of neuronal cells. In addition, Slit2 inhibits migration of endothelial cells through Robo4 [7]. On the basis of these published observations, it is reasonably speculated that Robo4 signaling inhibits HSC migration. It was also reported that *Drosophila* Slit/Robo signaling inhibits N-cadherin function in mammalian cells [29]. Since N-cadherin has been shown to play critical roles in the adhesion of HSCs and osteoblasts in the BM niche [9, 13], we also speculated that Robo4/Slit2 signaling might regulate HSC-osteoblast interaction upon myelosuppression. However, our preliminary analysis indicated that Slit2 did not inhibit migration of KSL cells toward SDF-1, and Robo4/Slit2 signaling did not inhibit N-cadherin-mediated adhesion in mammalian cells (unpublished observation). These data do not necessarily exclude the possibility that Robo4/Slit2 system is involved in migration or adhesion of HSCs in the physiological settings, and additional studies using gene-deficient animals will be required to unravel the precise roles of Robo4/Slit2 signaling in the HSC dynamics.

In a similar vein as the regulation of HSCs by the BM niche, it is intriguing that enhanced Slit2/Robo4 signaling resulted in the decreased residence of HSCs in the SP fraction. The SP phenotype is defined as a cell population with a high capacity of Hoechst 33342 dye efflux, and the efflux of Hoechst dye is accomplished by one of the ATP-binding cassette transporters, ABCG2/Bcrp-1 [30]. A gene disruption study in mice revealed that Bcrp-1 is absolutely required for the SP phenotype [31]; however, the expression of Bcrp-1 is equally observed in SP and non-SPs of $CD34^-KSL$ cells, suggesting that the function of Bcrp-1 is regulated by other factors [32]. Our finding that enhanced Slit2/Robo4 signaling led to decreased HSC residence in the SP fraction indicates that Slit2 could be a candidate factor regulating the Bcrp-1 function. In this regard, the induction of Slit2 in osteoblasts upon myelosuppression is of particular interest. It has been reported that HSCs are recruited from the SP to the non-SP fraction on days 4–6 after 5-FU treatment [13]. The induction of Slit2 occurs on days 3–6 after 5-FU administration, which precedes or coincides with the SP to non-SP transition of HSCs. These data suggest that Slit2 induced in the BM niche upon myelosuppression acts on HSCs through Robo4 and may play a critical role in their transition from the SP to the non-SP fraction. Preliminary analysis of Robo4-deficient mice showed that there is only a slight difference, if any, in the proportion of KSL-SP cells between knockout and wild-type animals (data not shown). This suggests that other redundant pathways, in addition to Robo4, could regulate the SP to non-SP transition of HSCs, and further detailed analysis of Robo4-deficient mice would be required to unravel precise roles of Robo4 in vivo. Considering a well-recognized role of Robo/Slit signaling in cellular migration [1], it is also tempting to speculate that Slit2 might be acting to induce HSC migration out of the niche in response to myelosuppression.

SUMMARY

We identified Robo4 as a receptor expressed on hematopoietic stem cells that is potentially involved in the regulation of the SP phenotype. Revealing the physiological role of Robo4/Slit2 signaling would lead to a better understanding of HSC homeostasis in the BM niche.

ACKNOWLEDGMENTS

We thank N. Watanabe, T. Shibata, and S. Saito (FACS Core Laboratory, Institute of Medical Science, University of Tokyo) for FACS sorting, and Dr. Dovie R. Wylie for language assistance. This work was supported in part by a grant from the Ministry of Education, Culture, Sports, Science and Technology of Japan. H.N. is currently affiliated with the Division of Hematology, Department of Internal Medicine, Keio University School of Medicine, Tokyo, Japan.

DISCLOSURE OF POTENTIAL CONFLICTS OF INTEREST

J.P.H. was employed by R&D Systems.

REFERENCES

1 Wong K, Park HT, Wu JY et al. Slit proteins: Molecular guidance cues for cells ranging from neurons to leukocytes. Curr Opin Genet Dev 2002;12:583–591.

2 Rajagopalan S, Nicolas E, Vivancos V et al. Crossing the midline: Roles and regulation of Robo receptors. Neuron 2000;28:767–777.

3 Brose K, Bland KS, Wang KH et al. Slit proteins bind Robo receptors and have an evolutionarily conserved role in repulsive axon guidance. Cell 1999;96:795–806.

4 Wu JY, Feng L, Park HT et al. The neuronal repellent Slit inhibits leukocyte chemotaxis induced by chemotactic factors. Nature 2001;410:948–952.

5 Wang B, Xiao Y, Ding BB et al. Induction of tumor angiogenesis by Slit-Robo signaling and inhibition of cancer growth by blocking Robo activity. Cancer Cell 2003;4:19–29.